Journal of Chemical Health Risks

www.jchr.org

JCHR (2024) 14(4), 456-465 | ISSN:2251-6727

A Comparative Study of Removal of CR(III) from Contaminated Water Using Ribose, Valine and Their Mixture as Facilitating Agents on Selected Adsorbents

Sreedhar Kodiganti[1,2], Abhijit Kantankar[2], Sreekantha B. Jonnalagadda[3] and Chandra Sekhar Vasam[1*].

[1]Department of Chemistry Pharmaceutical Chemistry, Telangana University Nizamabad-503322, India.

[2]Department of Chemistry, Tara Government College (A), Sangareddy-502001, India.

[3]School of Chemistry & Physics, University of KwaZulu-Natal, Durban, South Africa.

(Received: 14 April 2024 Revised: 1 May 2024 Accepted: 18 June 2024)

KEYWORDS

Adsorption of Cr(III), Complexing ligands, Metal-ligand complexes, CNP, Clay adsorbents.

ABSTRACT:

Adsorption of Cr(III) and Cr(III)-ligands (ribose and valine) on selected adsorbents Celite, Bentonite, Cellulose, Activated carbon (AC), and Carbon Nanoparticles (CNP) studies showed that clay-based materials and cellulose poorly adsorbed the Cr(III). Conversely, carbon adsorbents exhibited increased adsorption for Cr(III) complexed with ligands. Notably, carbon nanoparticles (CNP) remained the most efficient adsorbent (867.05 ppm) with valine complexed Cr(III), suggesting its porous structure could accommodate the larger complex. The Cr(III)-ribose-valine complex displayed an intermediate adsorption capacity, implying the smaller valine ligand partially counteracts the steric effect caused by ribose. XRD analysis confirmed the formation of crystalline structures for all Cr(III)-CNP and Cr(III)-ligand complexes. SEM images provided visual evidence for stronger interactions between the CNP and metal and metal-ligand complexes. TGA-DTA revealed a multi-step decomposition process for the Cr(III)-ligand complexes, with complete removal around 670°C, suggesting a well-defined crystalline structure between Cr(III) and both ligands. Complexation of Cr(III) with ligands significantly increases its adsorption on various materials. While clay and cellulose are less effective, carbon adsorbents offer some degree of adsorption even with the bulky complex. The size and geometry of the complex play a crucial role in its adsorption behaviour.

1.0. Introduction:

Chromium is a fairly common element, ranking the 21st most abundant element in earth's crust, at around 100 parts per million (ppm). Globally, 80% of mined chromium is used in metallurgical applications and 15% in chromium chemicals]1]. It's found naturally in rocks [2], soil [3], volcanic ash [4], and even living things [5]. It occurs mainly in chromite ore ($FeCr_2O_4$), where chromium exists in the +3-oxidation state [1]. In water bodies, chromium occurs in the Cr^{+3} form or chromium hydroxide [$Cr(OH)_n^{(3-n)+}$]. When released into the air, Cr(III) becomes an aerosol. The amount of chromium varies depending on the location, but it typically ranges from 1 to 3000 milligrams per kilogram (mg/Kg) in soil, 5 to 800 micrograms per litre (µg/L) in seawater, and 26 µg/L in freshwater [6].

Majority of chromium ore reserves are concentrated in Kazakhstan (40%), South Africa (35%), and India (18%). India ranks third in global chromite production (10%), following South Africa (46%) and Kazakhstan (18%) [7].

Thermodynamically, the Cr(III) is the most stable and has numerous compounds. Kinetically, these compounds have stability due to the half-filled configuration of chromium in the t2g level with d3 configuration, which gives it a preference for octahedral geometries [8]. Environmental regulations limit chromium in wastewater to 2 milligrams per litre (mg/L) for Cr(III) and only 0.5 mg/L for the more toxic Cr(VI) [9].

Journal of Chemical Health Risks
www.jchr.org
JCHR (2024) 14(4), 456-465 | ISSN:2251-6727

Cr(III), is an essential nutrient for humans, playing a role in metabolizing carbohydrates, fats, and proteins [10, 11]. A lack of Cr(III) can impair insulin function and protein synthesis, leading to decreased energy production, type-2 diabetes, and cardiovascular problems [10, 11]. The US Food and Drug Administration (FDA) recommends a daily reference intake (RDI) of 120 micrograms (µg) of chromium [12]. Dietary sources rich in Cr(III) include whole grains, high-bran cereals, egg yolks, coffee, nuts, green beans, broccoli, meat, and Brewer's yeast [12, 13]. At high concentrations, long-time exposure to Cr(III) causes detrimental effects on human health [14].

Cr(III) compounds have remarkable stability. They resist oxidation and reduction under normal conditions, making them valuable for various applications. One of the main properties of Cr(III) is its high melting point, and combined with its excellent corrosion resistance due to a self-passivating oxide layer [15, 16], makes it suitable for steel [17], Metal plating [18], Heat-resistant alloys [19] and Refractory materials [20]. Cr(III) often exhibits colour, lending itself (in the salt form) to pigments used in ceramics, glass, and paints [21]. Cr(III) is used in the tanning process in the leather industry, resulting in more durable and decay-resistant leather [22]. Cr(III) compounds act as catalysts to accelerate organic compound synthesis [23].

While Cr(III) (Cr(III)) has many beneficial applications, its widespread use can lead to environmental contamination [24]. Cr(III) released into water, air, and soil can harm plants and animals. Although not essential for plants, Cr(III) can be toxic. It can stunt plant growth by reducing root and shoot length and leaf number [24]. It disrupts physiological and biochemical processes, ultimately impacting crop yield and productivity [24]. Similarly, the presence of chromium can also inhibit the growth of algae, fungi, and bacteria [25].

Chromium enters the body through the lungs and gastrointestinal tract. However, the two forms of chromium have very different absorption rates. Cr(III) is poorly absorbed by the body, while Cr(VI) is readily taken in [26]. Even ingested Cr(VI) is converted to Cr(III) before entering the bloodstream, but this process involves reactive chromium intermediates that can damage cells. These effects, along with changes in gene regulation, contribute to the toxic, mutagenic, and cancer-causing properties of Cr(VI) [26]. While moderate amounts of chromium are beneficial, excessive dietary intake of Cr(III) can still be harmful. Overconsumption may lead to low blood sugar, liver damage, kidney problems, nerve damage, and irregular heartbeat [27]. For fish living in chromium-contaminated water, the story is different. Cr(III) itself isn't a major concern, and is an essential component of different enzymes, but Cr(VI) is highly toxic. Exposed fish experience loss of balance, restlessness, reduced breathing, increased mucus production, anaemia, and damage to internal organs like gills, liver, kidneys, and intestines [28].

Removing Cr(III) from various effluents is an ongoing challenge that requires continued development of new technologies. In wastewater treatment, adsorption may be one of the most popular methods due to its ease of use, selectivity, and effectiveness [29]. However, other promising methods exist, including membrane filtration, chemical precipitation, ion exchange, and electrochemical techniques like electrocoagulation, reduction, electrodialysis, and electrodeionization. Additionally, photocatalysis and nanotechnology offer possibilities for Cr(III) removal [30].

Metal ions react with ligands in aqueous solutions to form Metal-Ligand Complexes (MLCs) [31] and have different stereochemistry due to differences in sizes and charges around the central metal ion. On an adsorbent, the MLCs show adopted adsorption compared to metal ions due to their difference in solubility in solvent and interactions with the adsorbent. In this study, we compared the adsorption of MLCs with Metal ions on selected adsorbents, such as Bentonite, Celite, Cellulose, Activated Carbon, and CNP, using Valine (Val), Ribose (Rib) and their mixture. Cr(III)-Ligand Complexes (CrLCs) were prepared and validated with the recordings of FTIR spectra. The values of Atomic Absorption Spectra (AAS) gave the extent of adsorption of CrLCs on adsorbents.

2.0. Experimental:

2.1. Preparation of Cr(III)-Ligand Complexes:

All chemicals used were analytical grade. Cr(III) chloride hexahydrate is the starting material for preparing Cr(III)-ligand complex solutions. Three separate complex solutions were prepared in water at

Journal of Chemical Health Risks
www.jchr.org
JCHR (2024) 14(4), 456-465 | ISSN:2251-6727

room temperature using a 1:2 molar ratio (metal ion to ligand). The ligands employed were D-ribose (a sugar molecule), D-valine (an amino acid) and A 1:1 molar ratio mixture of D-ribose and D-valine. The solutions were stirred continuously for 5 hours to ensure complete complex formation between the Cr(III) ions and the respective ligands.

2.2. Adsorption Experiments:

For each Cr(III)-ligand complex, 10 mL aliquots were mixed with 5 grams of each elite, Bentonite (clay minerals), Cellulose (a polysaccharide), Activated Carbon (AC), and Carbon Nanoparticles (CNP) and transferred to separate flasks. The mixtures were then allowed to interact for 48 hours under controlled conditions to facilitate the adsorption of the Cr(III)-ligand complexes onto the surfaces of the adsorbents. The Cr(III)-ligand complexes were separated from the solutions using filtration, washed with dilute nitric acid, and cleaned by rinsing with distilled water to remove residual acid traces. Finally, the washed complexes were dried in an oven at 60°C for 10 hours to remove any remaining moisture.FTIR (Fourier Transform Infrared) spectroscopy analysis on the isolated Cr(III)-ligand complexes was performed to confirm the successful formation of complexes between the Cr(III) ions and the respective ligands. The appearance of specific functional group peaks in the FTIR spectra will provide evidence for complexation.

2.3. Evaluation of Adsorption:

The amount of iron (Cr(III)) adsorbed onto the various adsorbents was quantified using Atomic Absorption Spectroscopy (AAS). It measures a specific wavelength of light absorbed by the metal. For Cr(III), a characteristic wavelength is 357.9 nm. The AAS measurements provided the weight of Cr(III) adsorbed onto each adsorbent for all three Cr(III)-ligand complex solutions (Cr(III)-Val, Cr(III)-Rib, and Cr(III)-Rib-Val mixture). The results will show which complex and adsorbent combination exhibited the highest adsorption capacity.

2.4. Further characterization: Using X-ray diffraction (XRD) and energy-dispersive X-ray spectroscopy (EDS), the crystal structures and elemental compositions of Cr(III)-Val, Cr(III)-Rib complexes, and Cr(III)-Rib &val mixture were analyzed. Scanning electron microscopy (SEM) was used to examine the surface morphology of the Cr(III) complexes adsorbed on different adsorbents.

3.0. Results and Discussion:

3.1. AAS Analysis of adsorption of Cr(III) on various adsorbent with and with and

without ligands:

Table. 1. AAS values for adsorption of Cr(III) on adsorbents with and without ligands

Sl. No.	Adsorbent	Ligand	AAS in ppm
1	Celite	Without ligand	119.36
2		Ribose	120.18
3		Valine	134.08
4		Ribose and valine	128.80
5	Bentonite	Without ligand	246.87
6		Ribose	245.60
7		Valine	238.16
8		Ribose and valine	358.43

Journal of Chemical Health Risks
www.jchr.org
JCHR (2024) 14(4), 456-465 | ISSN:2251-6727

9	Cellulose	Without ligand	110.54
10		Ribose	114.27
11		Valine	217.42
12		Ribose valine	139.46
13	Activated Carbon	Without ligand	331.23
14		Ribose	383.59
15		Valine	685.37
16		Ribose and valine	461.00
17	CNP	Without ligand	753.12
18		Ribose	798.00
19		Valine	857.05
20		Ribose and valine	840.62

The Atomic Absorption Spectroscopy (AAS) studies revealed insights into how the presence of ribose and valine ligands affect Cr(III) adsorption on various adsorbents (Table. 1). Compared to Cr(III) alone, the Cr(III)-rib complex did not significantly alter the adsorption of Cr(III) on clay-based adsorbents (Celite and Bentonite) and cellulose. It suggests that the bulky Cr(III)-ribose complex might be too large to be effectively fit within pores or active sites in these materials. However, the adsorption increased to some extent for carbon adsorbents, AC and CNP (Fig. 1).

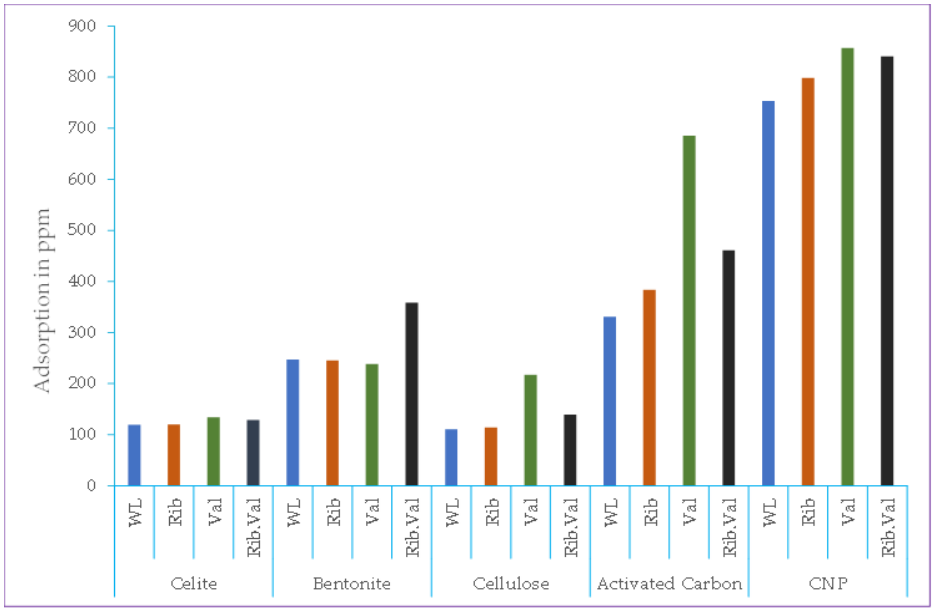

Fig. 1. Adsorption of Cr(III) with and without ligands on various adsorbents

Journal of Chemical Health Risks
www.jchr.org
JCHR (2024) 14(4), 456-465 | ISSN:2251-6727

Interestingly, there was an opposite trend for carbon-based adsorbents, i.e., activated carbon (AC) and CNP. These adsorbents displayed increased adsorption of chromium when complexed with ribose and valine. This behaviour can likely be due to the highly porous nature of AC and CNP, which allows better access to the larger complex, leading to higher adsorption.

Furthermore, the study revealed CNP (867.05 ppm) as the most effective adsorbent for Cr(III) removal, followed by AC (685.37 ppm). It aligns with previous findings suggesting that the high porosity of these materials plays a crucial role in their adsorption capacity. The experiment also investigated complexes containing a mixture of ribose and valine ligands (Cr(III)-Ribose-Valine). These complexes displayed an intermediate adsorption capacity between CNP (840.62 ppm) and AC (461.00 ppm), falling between the values observed for the individual ribose and valine complexes. It implies that the smaller valine ligand alongside ribose might partially counteract the steric hindrance effect, allowing for some improvement in adsorption compared to the pure Cr(III)-ribose complex.

3.2. Analysis of FTIR spectra of Cr(III)-ligand complexes:

Fourier-Transform Infrared Spectroscopy (FTIR) analysis provided strong evidence for the formation of coordination complexes between Cr(III) and the studied ligands (ribose and valine). Figure 1 visually depicts the spectral changes observed.

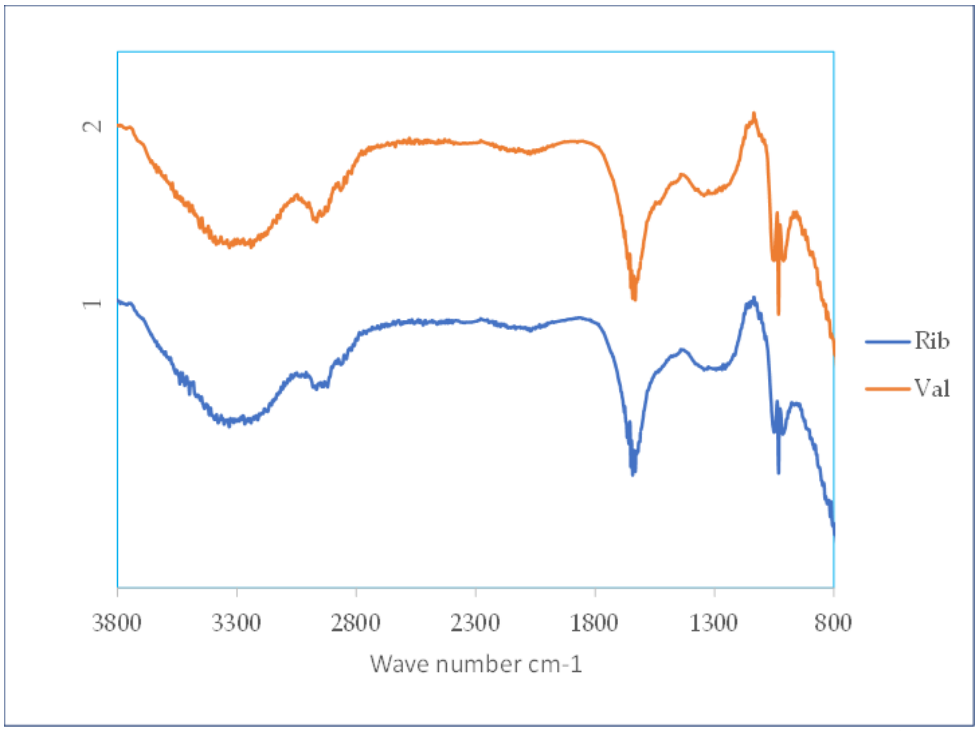

Fib. 2. FTIR spectral analysis of Cr(III)-Rib and Cr(III)-Val complexes

3.2.1. Ribose Complex: The spectrum of the Cr(III)-ribose complex (Fig. 2, Curve 1) shows the disappearance of several characteristic peaks compared to free ribose. These missing peaks, typically observed around 1332, 1275 cm^{-1} (O-H bending), 1010, 1030 cm^{-1} (C-O-C stretching), and 725, 820 cm^{-1} (C=C bending), indicate the involvement of these functional groups in complex formation with iron(III). New peaks appear at 1030, 1632, 2964, 1222-1363, and 3170-3375 cm^{-1}. Further analysis for the definitive assignment of these new peaks suggests potential interactions between the ligand and the metal centre.

3.2.2. Valine Complex:

The Cr(III)-valine complex (Fig. 2, Curve 2) has also obtained similar results. The spectrum displays a

Journal of Chemical Health Risks
www.jchr.org
JCHR (2024) 14(4), 456-465 | ISSN:2251-6727

disappearance of characteristic peaks associated with valine, including those around 2624 cm^{-1} (N-H stretching in carboxylic acid), 1509 cm^{-1} (NH3 bending), 1064 cm^{-1} (NH3 rocking), and 1578, 1139 cm^{-1} (asymmetric and symmetric COO stretching, respectively). This disappearance suggests the involvement of these functional groups in coordinating with Cr(III). Furthermore, new peaks emerge at 1032, 1631, 2966, 3172-3358, and 1250-1328 cm^{-1}. These new and the disappearance of the original signals provide strong evidence for the existence of a coordination complex between Cr(III) and valine.

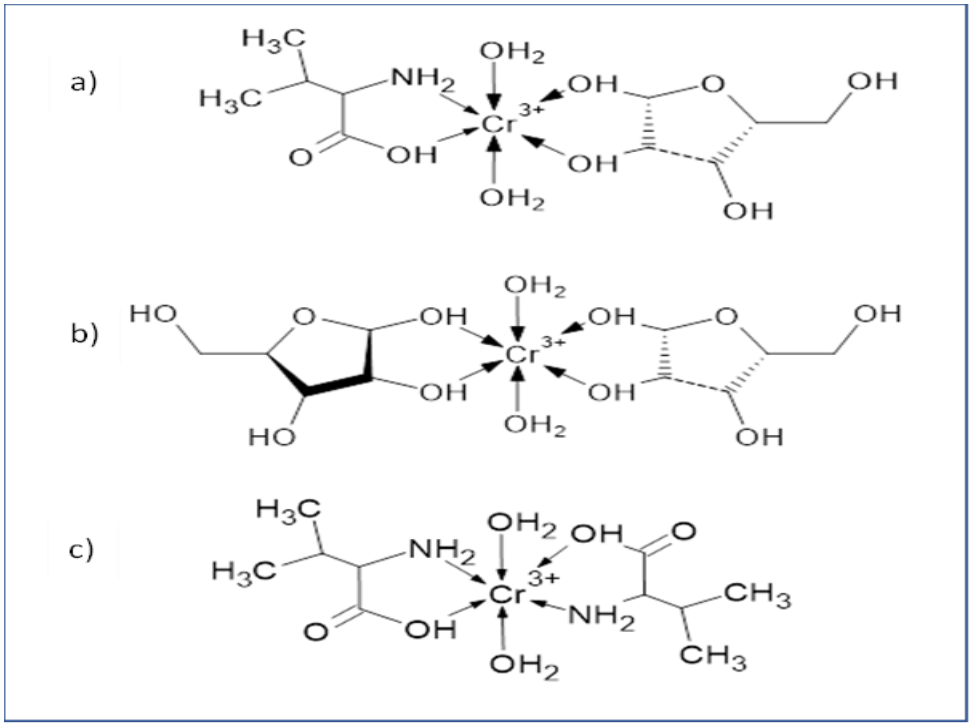

Fig. 3. a) Cr(III)-Valine b) Cr(III)-ribose, and c) Cr(III)-Val & Rib

The FTIR analysis confirms a dative bond between Cr(III) and the chosen ligands (ribose and valine) in a complex. By identifying changes in the characteristic peaks of the free ligands, we can infer the functional groups involved in coordinating with the metal centre. The structures of Cr(III)-Ligand complexes are shown in Fig. 3.

4.0. X-ray Diffraction (XRD) Analysis of Cr(III)-CNP Complexes:

X-ray diffraction (XRD) was employed to investigate the crystal structures formed between Cr(III) and CNP, as well as between Cr(III) complexes containing ribose or valine ligands and CNP. The XRD spectra were recorded in ASCII-2Theta-Intensity (.ASC) format, covering a range of 2θ angles from 9.9940° to 89.9790°.

The analysis revealed the presence of crystalline phases in all three samples: Cr(III)-CNP (Fig. 5a), Cr(III)-ribose complex adsorbed on CNP (Fig. 5b), and Cr(III)-valine complex adsorbed on CNP.

4.1. Cr(III)-CNP: The spectrum for Cr(III)-CNP (Fig. 4a) exhibits sharp peaks at 26.52° (with the highest relative intensity of 100%), 42.72°, and 22.75°, indicating a well-defined crystal structure between Cr(III) and CNP.

4.2. Cr(III)-Ribose-CNP: The presence of the Cr(III)-ribose complex adsorbed onto CNP (Fig. 4b) is confirmed by distinct signals at 26.50° (most intense peak), 43.86°, and 54.63°, along with other less prominent peaks. These unique peak positions differ slightly from those observed for Cr(III)-CNP alone, suggesting a distinct crystal structure for the adsorbed complex.

Journal of Chemical Health Risks
www.jchr.org
JCHR (2024) 14(4), 456-465 | ISSN:2251-6727

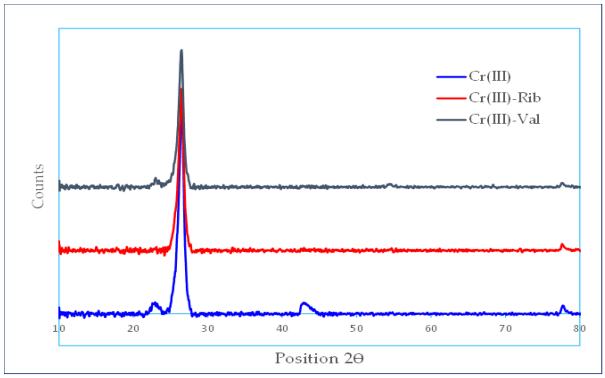

Fig 4. XRD of a) Cr(III), b) Cr(III)-Rib, and c) Cr(III)-Val on CNP

4.3. Cr(III)-Valine-CNP: Similarly, the spectrum for Cr(III)-valine adsorbed on CNP (Fib. 4c) shows peaks at 26.46° (most intense), 22.98°, and 77.64°, accompanied by additional signals. This distinctive peak pattern provides evidence for the formation of crystals involving the Cr(III)-Val-CNP complex.

5.0. SEM images of Cr(III)-Ligand complexes in comparison with Cr(III) ions on CNP

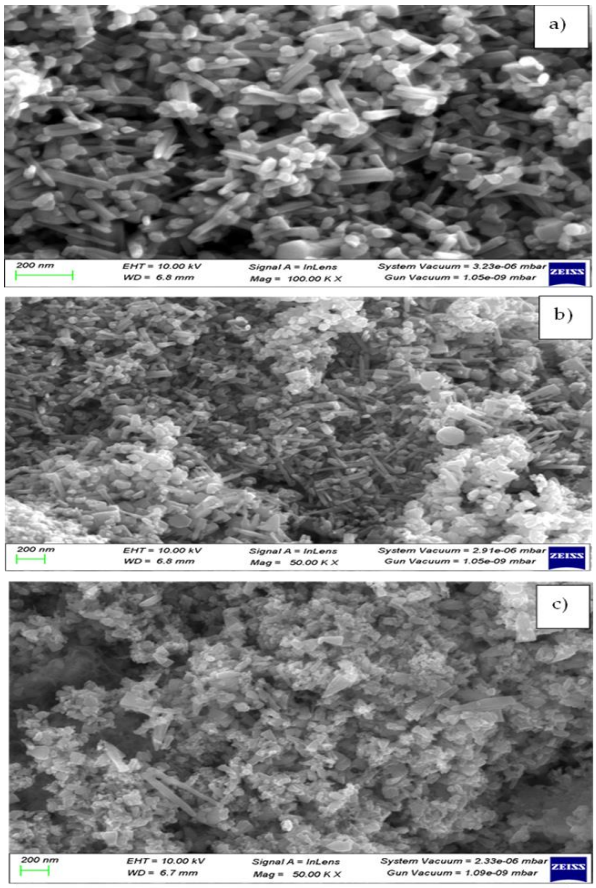

Fig. 5. SEM images of a) Cr(III), Cr(III)-Ribose and c) Cr(III)-Valine complexes

Scanning Electron Microscopy (SEM) analysis provided a powerful tool to directly visualize the adsorption process of Cr(III) onto the CNP surface. It offered valuable insights into the distribution and extent of the adsorbed species. Figure 5 presents SEM images for three samples: (a) CNP with adsorbed Cr(III) only, (b) CNP with Cr(III) complexed with riboflavin (Cr(III)-Rib), and (c) CNP with Cr(III) complexed with valine (Cr(III)-Val). In these images, the presence of white patches on the CNP surface signifies the adsorbed material. Notably, the white patches in Figure 5a appear to cover a significantly lower surface area compared to those in Figures 5b and 5c. This suggests a greater extent of adsorption for Cr(III) complexed with ribose and valine. Interestingly, Figure 5c shows the highest coverage, indicating the strongest adsorption for the Cr(III)-Val complex.

6.0. TGA and DTA analysis for Cr(III)-ligand (ribose and valine) complexes:

Thermogravimetric analysis (TGA) and differential thermal analysis (DTA) are powerful techniques used to investigate the physical and chemical changes that occur during the interaction of ligands with metal ions and the subsequent adsorption of the formed complexes onto adsorbent materials.

6.1. Cr(III)-Ribose complex:

Figure 6 depicts the decomposition and desorption process of chromium-ribose (Cr-Rib) complexes adsorbed onto CNP adsorbent.The TGA curve reveals several events. The initial weight loss of 8.26% observed at around 200°C corresponds to the evaporation of volatile substances and water molecules crystallized within the complex. Interestingly, the DTA curve indicates that this desorption process is exothermic. The peak exothermic event occurs at 449.15°C, coinciding with a significant weight loss of 56.14%, and suggests the desorption of a substantial portion of the Cr-Rib complex from the CNP adsorbent.

The analysis further reveals the thermal stability of the remaining complex. Up to 562.34°C, the weight change remains minimal, indicating a stable complex. However, a significant weight loss (83.91%), suggests the desorption of most of the remaining ribose molecules from the chromium. Finally, at 673°C, complete desorption of the Cr-Rib complex is achieved.

Journal of Chemical Health Risks
www.jchr.org
JCHR (2024) 14(4), 456-465 | ISSN:2251-6727

It's important to note that the TGA curve shows a final weight percentage exceeding 100% (104.684%) at 748.69°C. This can be attributed to the decomposition of the CNP adsorbent itself at high temperatures.

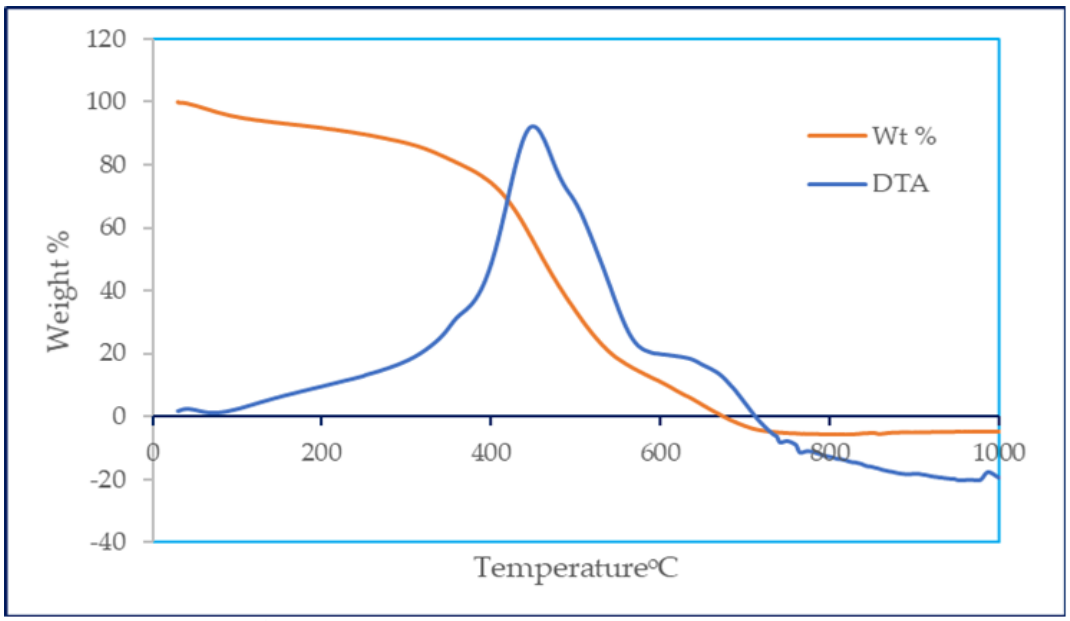

Fig.6. TGA and DTA of Cr-Ribose complex

6.2. Cr(III)-Ligands complex: For Cr(III)-Ligands (Ribose and Valine), (Fig. 7)the first weight loss, around 5.62% at 200°C, corresponds to the evaporation of volatile materials and water molecules trapped within the crystal structure.

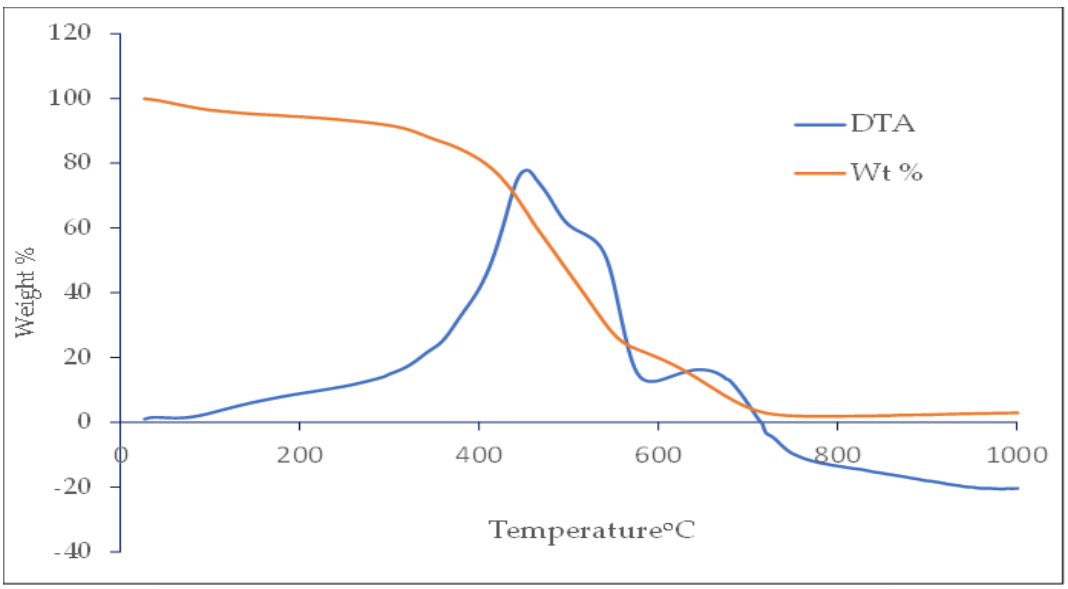

Fig.7. TGA and DTA of Cr-ligands (Rib and Val)compl

This initial process is also exothermic, and the temperature rises to 453.61°C. The most significant weight loss, 76.5%, occurs at the end temperature of 571.33°C, the desorption of ribose molecules. It's worth noting that this value was even higher, at 83.91% for chromium-ribose crystal. The second desorption event,

Journal of Chemical Health Risks

www.jchr.org

JCHR (2024) 14(4), 456-465 | ISSN:2251-6727

also exothermic as shown by DTA, happens at a higher temperature, reaching 647.22°C. This next stage is associated with the loss of valine molecules, resulting in a weight loss of 20.49% at 717.44°C. Overall, the experiment observed a total weight loss of 97.004%.These findings from the TGA analysis suggest a well-defined crystal structure between chromium (III) ions and the ligands, ribose and valine. This study demonstrates that incorporating complexing ligands onto clay and carbon adsorbents significantly enhances Cr(III) adsorption. As expected, carbon adsorbents, AC and CNP exhibited higher adsorption capacity than clay adsorbents, celite and bentonite. Further, cellulose showed the lowest adsorption. These findings highlight the effectiveness of complexing ligands in promoting heavy metal removal, facilitating their elimination from contaminated water.

Conclusions:

Organic molecules like ribose and valine helped chromium (III) to adsorb better on carbon-based materials (AC, CNP) compared to clay-based materials (Celite, Bentonite) and cellulose. Among the tested materials, CNP removed the most chromium (III) (867.05 ppm), followed by AC (685.37 ppm), because their pore structures were better suited for these complexes than just chromium (III) alone. The amino acid valine, with its functional groups NH2 and COO, bonded with chromium (III) more effectively than the hydroxyl groups of the sugar ribose. It was confirmed by the disappearance of peaks related to NH2 and COO in the ribose's spectral data, indicating the involvement of those groups in bonding with chromium (III). Similarly, the disappearance of signals for function groups and the appearance of new signals confirmed the formation of the Cr(III)-valine complex. X-ray diffraction analysis (XRD) confirmed the crystalline nature of the chromium (III) complexes with CNP, ribose-CNP, and valine-CNP. The organic molecules (ribose and valine) influenced how the chromium (III) and CNP arranged themselves in the crystal lattice, resulting in unique crystalline structures for each complex. Analysis using thermogravimetric analysis (TGA) and differential thermal analysis (DTA) indicated that chromium (III) forms very stable complexes with ribose and valine, stable up to 674°C. Electron microscope images (SEM) showed that chromium (III) complexes with ribose and valine adsorbed on CNP more extensively than chromium (III) alone. The chromium (III)-val complex showed the highest adsorption. The similar results in the AAS studies confirm it. This research paves the way for new methods to remove heavy metals from polluted water using designed remediation techniques that involve ligands.

References:

1. J. Barnhart, Occurrences, Uses, and Properties of Chromium, *Regulatory Toxicology And Pharmacology*, 26, S3-S7 (1917).
2. M.A. Torkmahalleh, L. Lin, T.M. Holsen, D.H. Rasmussen and P.K. Hopke, The impact of Deliquescence and pH on Cr Speciation in Ambient PM Samples, Aerosol Sci. Technol. 46(6), 690-690 (2012).
3. H. Cheng, T. Zhou, Q. Li, L. Lu and C. Lin, Anthropogenic Chromium Emission in China from 1990 to 2009, *PLos One,* 9(2), e87753 (2014).
4. I.F. Olmo. M. Puento and L. Montecalvo, Source contribution to the bulk atmospheric deposition of minor and trace elements in a Northen Spanish costal urban area, Atmos. Res. 145(80), 91 (2014).
5. R. Rupali, D. Leena and H.D. Juneja, Chemical Speciation of Chromium in Water: A Review, *Crit. Rev. Environ. Sci. Technol.*, 42 (7), 776-810 (2012).
6. Jacobs JA, Testa SM. Overview of chromium (VI) in the environment: background and history. In: Guertin, J.; Jacobs, JA. Avakian, CP., editors. Chromium (VI) Handbook. Boca Raton, Fl: CRC Press; p. 1-22 (2005).
7. Government of India, Ministry of Mines, Indian Bureau of mines, Indian Minerals Year Book 2020, 59, p. 6-13 (2022).
8. S.I. Shupack, The chemistry of Chromium and Some Resulting Analytical Problems, *Environ. Health Perspect.*, 92, 7-11 (1991).
9. D.T. Lamb, K. Venkataraman, N. Bolan, N. Aswanth, G. Choppala and R. Naidu, Pytocapping: an alternative technology for the sustainable management of landfill sites, *Crit. Rev. Environ. Sci. Technol.*, 44(6), 561-637 (2014).
10. Md. M. Uddin, Md.J. Hasan, Md. D. Islam, A. Rahaman and S. Md. Shamsuddin, Removal of Chromium (III) and Other Physical Parameters from Chrome Tan Wastewater and Recovery of Chromium from the Precipitating Sludge, *TLR*, 3(2), 64-77 (2020a).

Journal of Chemical Health Risks

www.jchr.org

JCHR (2024) 14(4), 456-465 | ISSN:2251-6727

11. J.B. Vincet, The bioinorganic chemistry of chromium(III), Polyhedron 20(1-2), 1-26 (2001).
12. A. Swaroop, M. Bagchi, H.G. Preuss, S. Zafra-Stone, T. Ahamad and D. Bagchi, The Benefits of chromium(III) complexes in animal and human health, The Nutritional Biochemistry of Chromium(III), p. 251-278 (2019).
13. A.P. Das and S. Mishra, Hexavalent Chromium (VI): Environment Pollutant and Health Hazard, *J. Environ. Res. Develop*, 2(3), 386-392 (2008).
14. F.J. Alguacil, The 2019 year review on chromium(III) adsorption of aqueous solutions, *Desalination and Water Treatment*, 201, 228-239 (2020).
15. B. Robert, B. Ulf, T.G. Mikael and H. Sven-Erik, A Comparative study of the corrosion protective properties of chromium and chromium free passivation methods, *Surface & Coating Technology*, 202, 391-397 (2007).
16. B. Sun, X. Zuo, X. Cheng and X. Li, The role of chromium content in the long-term atmospheric corrosion process, *Npj Materials Degradation*, 4, 37 (2020).
17. P.J. Anderson, 1.3.3B Stainless Steels, An Introduction to Materials in Medicine, Biomaterials Science (Fourth Edition) p. 249-255 (2020).
18. V.S. Protsenko, L.S. Bobrova, T.E. Butyrina and F.I. Danilov, Hydrogen evolution reaction on Cr-C Electrocatalysts Electrodeposited from a Choline Chloride based Trivalent Chromium Plating Bath, *Voprosykhimiiikhimicheskoitekhnologii*, pp. 61-66 (2019).
19. A.B. Olga, V.A. Lyudnuia, Y.V. Tamara and D.B. Boris, New high-temperature heat-resistant alloys on the basis of the Cr-Ti-C system, *Int J Refract Hard Met*, 17(4), 259-263 (1999).
20. T. Xu, Y. Xu, N. Liao, Y. Li and M. Nath, High-Temperature Chemical Stability of Cr(III) Oxide Refractories in the Presence of Calcium Aluminate Cement, *Materials*, 14, 6590 (2021).
21. L. Verger, D. Oliver, C. Mathieu, T. Nicolas, G. Rousse and C. Laurent, Synthesis properties and uses of chromium-based pigments from the Manufacture de Sevres, *J. Cult. Herit.*, 30, 26-33 (2018).
22. S. Murali, D. Aruna and J.R. Rao, Ultraefficient Tanning Process: Role of Mass Transfer Efficiency and Sorption Kinetics of Cr(III) in Leather Processing, *ACS Sustainable Chem. Eng.*, 7, 3875-3882 (2019).
23. M. Jacek, J. Dagmara, G. Barbara and D. Joanna, New chromium(III)-based catalysts for ethylene oligomerization, *Sci Rep,* 10, 16578 (2020).
24. A.K. Shanker, C. Carvantes, H. Loza-Tavera and S. Avudainayagam, Chromium toxicity in plants, *Environ. Int.*, 31, 739-753 (2005).
25. C. Cervantes, J. Campos-Carcia, S. Devars, F. Gutierrez-Corona,H. Loza-Tavera, J.C. Torres-Guzaman and R. Moreno-Sanchez, Interactions of chromium with microorganisms and plants. *FEMS Microbiol. Rev.*, 25, 335-347, (2001).
26. R. Shrivastava, R.K. Upreti, P.K. Seth and U.C. Chaturvedi, Effects of chromium on the immune system, *FEMS Immunology and Medicinal Microbiology*, 34, 1-7 (2002).
27. F. Chen, J. Ma, S. Akhtar, Z.I. Khan, K. Ahmad, A. Ashfaq, H. Nawaz and M. Nadeem, Assessment of chromium toxicity and potential health implications of agriculturally diversely irrigated food crops in the semi-arid regions of South Asia, *Agri. Water Manag.*, 272, 107833, (2022).
28. A. Bakshi and A.K. Panigrahi, A comprehensive review on chromium induced alternations in fresh water fishes, *Toxicol Rep.*, 5, 440-447 (2018).
29. L. Frolova and B. Blyuss, Investigation of Cr(III) adsorption in aqueous solution using bentonite, *Appl. Nanosci.*, 13, 5323-5333 (2023).
30. H. Peng and J. Guo, Removal of chromium from wastewater by membrane filtration, chemical precipitation, ion exchange, adsorption coagulation, electrochemical reduction, electrodialysis, electrodeionization, potocatalysis and nanotechnology: a review, *Environ Chem Lett.*, 18, 2055-2069 (2020).
31. J.F. Perez-Benito and X. Julian-Millan. Ligand substitution in chromium(III)-aqua complexes by L-histidine: kinetic resolution of two-long lived intermediates, *React. Kinet. Mech.Catal.*, 128, 1-22 (2019).